Tight focusing of laser light using a chromium Fresnel zone plate

V. V. KOTLYAR,[1,2] S. S. STAFEEV,[1,2,*] A. G. NALIMOV,[1,2] M. V. KOTLYAR,[2] L. O'FAOLAIN,[3,4,5] AND E. S. KOZLOVA [1,2]

[1]*Image Processing Systems Institute—Branch of the Federal Scientific Research Centre "Crystallography and Photonics" of the Russian Academy of Sciences, 151 Molodogvardeyskaya St., Samara 443001, Russia*
[2]*Samara National Research University, 34 Moskovskoye Shosse, Samara 443086, Russia*
[3]*SUPA, School of Physics and Astronomy of the University of St. Andrews, North Haugh, St. Andrews, KY16 9SS Scotland, UK*
[4]*Tyndall National Institute, Lee Maltings Complex, Dyke Parade, Cork, Ireland*
[5]*Centre for Advanced Photonics and Process Analysis, Cork Institute of Technology, Cork, Ireland*
**kozlova.elena.s@gmail.com*

Abstract: Using near-field scanning microscopy, we demonstrate that a 15-μm zone plate fabricated in a 70-nm chromium film sputtered on a glass substrate and having a focal length and outermost zone's width equal to the incident wavelength λ = 532 nm, focuses a circularly polarized Gaussian beam into a circular subwavelength focal spot whose diameter at the full-width of half-maximum intensity is FWHM=0.47λ. This value is in near-accurate agreement with the FDTD-aided numerical estimate of FWHM=0.46λ. When focusing a Gaussian beam linearly polarized along the *y*-axis, an elliptic subwavelength focal spot is experimentally found to measure FWHMx=0.42λ (estimated value FWHMx=0.40λ) and FWHMy=0.64λ. The subwavelength focal spots presented here are the tightest among all attained so far for homogeneously polarized beams by use of non-immersion amplitude zone plates.

OCIS codes: (050.1380) Binary optics; (050.1965) Diffractive lenses; (050.6624) Subwavelength structures; (180.4243) Near-field microscopy; (260.5430) Polarization.

References

1. Y. Fu and W. Zhou, "Hybrid Au-Ag subwavelength metallic structures with variant periods for superfocusing," J. Nanophotonics **3**, 033504 (2009).
2. Y. Fu, R.G. Mote, Q. Wang, and W. Zhou, "Experimental study of plasmonic structures with variant periods for sub-wavelength focusing: analyses of characterization errors," J. Mod. Opt. **56**(14), 1550-1556 (2009).
3. R.G. Mote, S.F. Yu, A. Kumar, W. Zhou, and X.F. Li, "Experimental demonstration of near-field focusing of a phase micro-Fresnel zone plate (FZP) under linearly polarized illumination," Appl. Phys. B **102**, 95-100 (2011).
4. R.G. Mote, S.F. Yu, W. Zhou, and X.F. Li, "Subwavelength focusing behavior of high numerical-aperture phase Fresnel zone plates under various polarization states," Appl. Phys. Lett **95**, 191113 (2009).
5. Y. Fu, W. Zhou, L.E.N. Lim, C.L. Du, X.G. Luo, "Plasmonic microzone plate: Superfocusing at visible regime," Appl. Phys. Lett. **91**, 061124 (2007).
6. V.V. Kotlyar, S.S. Stafeev, Y. Liu, L. O'Faolain, A.A. Kovalev, "Analysis of the shape of a subwavelength focal spot for the linearly polarized light," Appl. Opt. **52**, 330-339 (2013).
7. S.S. Stafeev, V.V. Kotlyar, L. O'Faolain, "Subwavelength focusing of laser light by microoptics," J. Mod. Opt. **60**(13), 1050-1059 (2013).
8. T. Wang, X. Wang, C. Kuang, X. Hao, X. Liu, "Experimental verification of the far-field subwavelength focusing with multiple concentric nanorings," Appl. Phys. Lett. **97**(23) 231105 (2010).
9. P. Venugopalan, Q. Zhang, X. Li, L. Kuipers, M. Gu, "Focusing dual-wavelength surface plasmons to the same focal plane by a far-field plasmonic lens," Opt. Lett. **39**, 5744-5747 (2014).
10. K.R. Chen, W.H. Chu, H.C. Fang, C.P. Liu, C.H. Huang, H.C. Chui, C.H. Chuang, Y.L. Lo, C.Y. Lin, H.H. Hwung, A.Y.G. Fuh, "Beyond-limit light focusing in the intermediate zone," Opt. Lett. **36**, 4497-4499 (2011).
11. Y. Liu, H. Xu, F. Stief, N. Zhitenev, M. Yu, "Far-field superfocusing with an optical fiber based surface plasmonic lens made of nanoscale concentric annular slits," Opt. Express **19**, 20233-20243 (2011).
12. W. Song, Z. Fang, S. Huang, F. Lin, X. Zhu, "Near-field nanofocusing through a combination of plasmonic Bragg reflector and converging lens," Opt. Express **18**, 14762-14767 (2010).
13. D. Feng, "3D confinement of the focal spot of plasmonic Fresnel zone plate lens using gold bowtie nanoantenna," J. Opt. Soc. Am. A **31**, 2070-2074 (2014).

14. H. Wang, Y. Deng, J. He, P. Gao, N. Yao, C. Wang, X. Luo, "Subwavelength light focusing of plasmonic lens with dielectric filled nanoslits structures," J. Nanophotonics **8**(1), 083079 (2014).
15. M. Zhang, J. Du, H. Shi, S. Yin, L. Xia, B. Jia, M. Gu, C. Du, "Three-dimensional nanoscale Far-field Focusing of Radially Polarized Light by Scattering the SPPs with an Annular Groove," Opt. Express **18**, 14664-14670 (2010).
16. J. Ji, Y. Meng, L. Sun, X. Wu, J. Wang, "Strong Focusing of Plasmonic Lens with Nanofinger and Multiple Concentric Rings Under Radially Polarized Illumination," Plasmonics **11**(1), 23-27 (2015).
17. R. Peng, X. Li, Z. Zhao, C. Wang, M. Hong, X. Luo, "Super-Resolution Long-Depth Focusing by Radially Polarized Light Irradiation Through Plasmonic Lens in Optical Meso-field," Plasmonics **9**(1), 55-60 (2014).
18. E.S. Kozlova, V.V. Kotlyar, A.G. Nalimov, "Comparative mod-eling of amplitude and phase zone plates," Computer optics **39**(5), 687-693 (2015).
19. W. Ting, A.Y. Zhu, M. Khorasaninejad, Z. Shi, V.Sanjeev, F. Capasso, "Immersion metalenses at visible wavelength for nanboscale imaging," Nano Lett. **17**, 3188-3194 (2017).
20. A.D. Rakic, A.B. Djurišic, J.M. Elazar, M.L. Majewski, "Optical properties of metallic films for vertical-cavity optoelectronic devices," Appl. Opt. **37**(22), 5271–5283 (1998).

1. Introduction

Although zone plates (ZP) have been known in optics for quite long, they still arouse an incessant interest on the part of researchers. With the photonic components becoming increasingly miniaturized, there has been a growth of interest in ZPs with near-surface focus. Here, both amplitude and phase ZPs can be employed. The ZPs fabricated on the basis of certain metals are referred to as surface plasmon-polariton ZPs or lenses (SPP-lenses). A ZP with ring radii of $r_n^2 = 2nf\lambda + n^2\lambda^2$ (f =1 μm, λ = 633 nm) synthesized in 50-nm silver/gold films sputtered on a quartz substrate has been numerically simulated using a FDTD-method [1]. A focal spot of subwavelength size FWHM=0.3λ was numerically demonstrated at distance z = 1.5 μm from the ZP, with the spot intensity being 1.4-times that of the incident beam. Similar ZPs of diameter 8 μm in a 100-nm gold film have been synthesized and experimentally characterized [2]. A focal spot of size FWHM = 1.7λ (λ = 633 nm) was observed on a near-field microscope Ntegra (NT-MDT, 100-nm resolution) at distance z = 1.6 μm from the ZP, with the theoretically estimated size being FWHM = 0.54λ [2]. Focusing a linearly polarized 633-nm beam by means of a Fresnel ZP with 0.5-μm focus has been numerically simulated and experimentally studied [3]. The experimentally measured elliptic focal spot was equal to FWHM = 0.63λ on the minor semi-axis. In the FDTD-aided simulation [4], obtaining a focal spot of size FWHM = 0.39λ was reported. Focusing a linearly polarized wave with an amplitude ZP of 0.5-μm focus has also been numerically simulated using Richards-Wolf formulae [4]. Superfocusing with a plasmonic microzone plate fabricated in a silver film applied on a glass substrate has been studied [5]. In the FDTD-aided simulation, a microzone plate was shown to generate a 0.33λ-nm focal spot. A phase ZP with a focal length of f = λ = 532 nm has been experimentally shown to produce a subwavelength elliptic focal spot measuring FWHMx = 0.44λ and FWHMy=0.52λ [6]. When illuminated by a different wavelength (λ = 633 nm), the ZP-aided spot became more oblong, measuring FWHMx = 0.40λ and FWHMy = 0.60λ [7], with the minor-axis size becoming smaller.

Plasmonic microlenses intended to focus evanescent surface waves often have a very simple structure in the form of a concentric ring array. For instance, an SPP lens composed of three concentric 300-nm annular slits in a Ge layer has been proposed [8]. The lens was shown to focus an incident wave λ into a subwavelength spot of size FWHM = 0.6λ. An SPP-lens composed of two con-centric rings of width 350 nm and depth 200 nm in a thin gold film for two wavelengths has been studied [9]. In a planar lens structured as three relief steps reported in [10], two outer V-shaped steps of total width 320 nm had a central slit of width and depth 80 nm. The central step was 320-nm wide and 120-nm deep. The structure was found to focus an incident wave λ into a subwavelength line of width FWHM = 0.34λ. An SPP-lens fabricated at an optic-fiber end was studied in two variants [11] – those composed of three and four concentric annular slits, with both having a 2.8-μm diameter and a 60-nm wide first slit. Focusing an incident 808-nm wave in a water solution enabled a

subwavelength focal spot of FWHM = 0.31λ to be observed. Near-field nanofocusing through the use of a combination of plasmonic Bragg reflector and converging lens has been reported [12], where two sets of concentric annular slits with different period were utilized. The inner part of the plasmonic lens was composed of 10 slits of period 640 nm, with the outer part containing nine slits of period 20 nm. Although in this way the light can be focused beyond the diffraction limit into a 0.31λ spot, on the negative side is that it was located just 80-nm away from the lens surface. In an interesting technique for subwavelength focusing described in [13] a tighter focal spot was attained by placing a bowtie nanoantenna in the focus of a plasmonic Fresnel lens. A varied-depth plasmonic lens fabricated of aluminum on a glass substrate has been proposed [14]. The lens for 3D confinement of light was simulated numerically, with its planar analog being fabricated and characterized by near-field scanning optical microscopy. As a result of 3D confinement, a focal spot of size FWHM=0.9λ was attained. When tightly focused, a linearly polarized beam generates an elliptic intensity distribution. For the focal spot to be radially symmetric, the incident light also needs to be symmetrically polarized. In particular, a radially polarized incident beam can be utilized. An SPP-lens for radially polarized light discussed in [15] was reported to produce a focal spot of size FWHM = 0.46λ (λ = 632.8 nm). An SPP-lens intended to focus a radially polarized light of wavelength 355 nm has been studied [16]. The numerical simulation was conducted in [16] using a finite difference FDTD method and a finite element method implemented using the COMSOL Multiphysics software. The lens under study was designed as a central nanofinger of diameter 45 nm surcirculared by 230-nm wide rings. The lens was fabricated in a 60-nm thick chromium film sputtered on a quartz substrate. Despite being fabricated, the authors have failed to discuss the results of focusing light using the said SPP-lens. Performance of an SPP-lens in a 405-nm silver layer was numerically simulated in [17]. The lens was also composed of concentric rings but was characterized by varied-depth grooves, leading to a variation in the focal length.

As the review above suggests, the majority of research has been purely theoretical. In most works, the focal spot size was larger than FWHM = 0.45λ. Meanwhile, where a tighter focal spot was reported to be attained, it was located very close to the surface, making it hardly accessible and with its maximal intensity being not higher than twice that of the incident light. In this work, we study a Fresnel ZP on a quartz glass both theoretically and experimentally, showing it to focus an incident linearly polarized beam into a subwavelength focal spot smaller than FWHM = 0.45λ. The propagation of a 532-nm beam was numerically simulated using a FDTD-method. The FDTD-aided simulation of a similar ZP conducted earlier [18] included the comparison of the performance of its amplitude and phase versions synthesized in chromium and silver films. It was shown that by taking into account dispersion of the material (quartz, silver, chromium) based on Selmeier and Drude-Lorentz dispersion models just insignificant changes (within 6%) in the focal spot parameters could be achieved. Note that the focal spots from the phase and amplitude ZP also changed in size only insignificantly, with the subwavelength spots varying from 0.41λ to 0.47λ. The major difference was that the focal spot intensity from the amplitude ZP was three times lower than that from the phase ZP.

In a recent paper [19], an immersion metalens with the numerical aperture NA=1.1, composed of an array of TiO_2 nanorods synthesized on a silica substrate was reported. When illuminated by a circularly polarized beam, the metalens formed a circular focal spot of size FWHM= 0.45λ.

In this work, we experimentally show that a simple non-immersion zone plate with NA=1 fabricated in a chromium film is able to focus a circularly polarized Gaussian beam, producing at a 600-nm distance a circular subwavelength focal spot of diameter FWHM= (0.47±0.02)λ. It is worth noting that while in [19] the nanorods were 600-nm high, the rings of the chromium zone plate reported here are just 70-nm high.

In this study, we additionally look into how the microrelief height affects the focal spot characteristics, showing that at the microrelief height of 60 nm and 80 nm it is possible to reach an optimal trade-off between the FWHM and the maximal intensity of the spot. We also conduct the numerical simulation of the performance of the fabricated ZP with a microrelief height of 67.5 nm (with an error of under 5%). Measurements on the near-field scanning optical microscope show that the fabricated ZP focuses a linearly polarized Gaussian incident beam into a subwavelength elliptic spot measuring FWHMx=0.42λ and FWHMy=0.64λ. For circular polarization, a near-circular focal spot measuring FWHMx=0.47λ and FWHMy=0.48λ is experimentally observed.

2. Numerical simulation results

The FDTD-aided (FullWAVE, RSoft) simulation looked into how the focal spot parameters and the maximal intensity were affected by the thickness of a chromium film in which the ZP was fabricated. The simulation parameters were as follows: wavelength – λ=532 nm, number of rings – 13, the outermost zone width (ridge plus indent) and the focal length were of wavelength size – 532 nm, and refractive index (Cr)- n=2.66+4.16i [20]. The computation was conducted at a λ/30 ≈ 20 nm step along the lateral coordinates, with the temporal step reduced to $c\Delta t$ = 7 nm. The incident Gaussian beam of 5-μm waist radius was circularly polarized. The simulation results are shown in Table 1.

Table 1. Parameters of the focal spot versus the relief height of a chromium ZP illuminated by a circularly polarized beam. The spot size was calculated in terms of half-maximum of the total intensity $I = I_x + I_y + I_z$.

h, nm	I_{max}, a.u.	$FWHM_x$, λ	$FWHM_y$, λ	DOF, λ	f, μm
20	6.9	0.528	0.531	0.752	0.598
30	8.9	0.550	0.552	0.787	0.580
40	10.0	0.564	0.567	0.805	0.577
50	10.7	0.569	0.573	0.815	0.577
60	11.1	0.567	0.573	0.821	0.577
70	11.2	0.565	0.570	0.824	0.570
80	11.2	0.56	0.567	0.825	0.555
90	11.1	0.557	0.564	0.823	0.555
100	10.9	0.555	0.562	0.822	0.555

From Table 1, the ZP is seen to generate at a 600-560-nm distance a near-circular focal spot of diameter FWHM=0.57λ, which is 10 percent larger than the diffraction limit of FWHM=0.51λ. Note that the maximal intensity of the focal spot, eleven times the incident light intensity, is attained at a chromium film thickness of 70 nm. For the sake of further discussion, note that the probe of a near-field scanning microscope only measures transverse intensity components, $I_\perp = I_x + I_y = |E_x|^2 + |E_y|^2$, being insensitive to the axial intensity component $I_z = |E_z|^2$. Assuming the 70-nm thickness of the chromium film and considering only the contribution of the transverse electric field components, we find that FWHM=0.461λ. Also, note that if we consider the focal-plane modulus of Poynting vector's projection onto the optical axis, $S_z \approx |\mathrm{Re}(E_x\bar{H}_y - \bar{E}_yH_x)|$, where Re denotes the real part of the number, H_x, H_y are projections of the magnetic field vector, and $\bar{A}$ is complex-conjugate to A, the size of the focal spot in terms of half-maximum $|S_z|$ is FWHM=0.456λ . This can be seen from Table 2 which presents results similar to those in Table 1, except that the focal spot size was calculated for $|S_z|$, i.e. the half-maximum of the projection of Poynting vector's modulus on the optical axis. It is worth noting that the focal spot sizes calculated in terms of $|S_z|$ and $I_\perp$ are very close to each other.

For the sake of completeness of this study, below are given the simulation results for the case when the ZP under study focuses a Gaussian beam E_y linearly polarized along the Y-axis. The data given in Table 3 are similar to those in Tables 1 and 2, except that the incident light

is linearly polarized and the spot size is evaluated in terms of half-maximum of the transverse intensity, $I_\perp = I_x + I_y$.

Table 2. Parameters of the focal spot versus the relief height of a chromium ZP illuminated by a circularly polarized beam. The spot size was calculated in terms of half-maximum of $|S_z|$.

h, nm	I_{max}, a.u.	$FWHM_x$, λ	$FWHM_y$, λ	DOF, λ	f, μm
20	6.9	0.474	0.475	0.752	0.598
30	8.9	0.463	0.465	0.787	0.580
40	10.0	0.457	0.457	0.805	0.577
50	10.7	0.456	0.457	0.815	0.577
60	11.1	0.456	0.457	0.821	0.577
70	11.2	0.456	0.457	0.824	0.570
80	11.2	0.462	0.462	0.825	0.555
90	11.1	0.464	0.465	0.823	0.555
100	10.9	0.467	0.467	0.822	0.555

Table 3. Parameters of the focal spot versus the relief height of a chromium ZP illuminated by a beam linearly polarized along the y-axis. The spot size was calculated in terms of the half-maximum of $I_\perp = I_x + I_y$

h, nm	I_{max}, a.u.	$FWHM_x$, λ	$FWHM_y$, λ	DOF, λ	f, μm
20	6.9	0.401	0.579	0.752	0.598
30	8.9	0.399	0.556	0.787	0.580
40	10.0	0.398	0.547	0.805	0.577
50	10.7	0.398	0.544	0.815	0.577
60	11.1	0.397	0.544	0.821	0.577
70	11.2	0.397	0.545	0.824	0.570
80	11.2	0.397	0.550	0.825	0.560
90	11.1	0.397	0.552	0.823	0.555
100	10.9	0.397	0.555	0.822	0.555

From Table 3, an elliptic focal spot generated at a 550-600-nm distance is seen to be 1.4 times larger along the *y*-axis when compared with the *x*-axis. As is the case in Tables 1 and 2, the focal intensity is maximal when the chromium film thickness is h=70 nm. In this case, the focal spot measures FWHMx=0.40λ and FWHMy=0.55λ.

Thus, in this section by rigorous numerical simulation we showed that a ZP in a 70-nm thick chromium film generates a focal spot of size, in terms of half-maximum $|S_z|$ or $I_\perp = I_x + I_y$, FWHM=0.46λ (circular polarization) or FWHMx=0.40λ and FWHMy=0.55λ (linear polarization).

3. Fabrication and modeling with regard for fabrication errors

The amplitude ZP was fabricated in chromium using e-beam lithography. The 15-μm ZP composed of 13 rings fabricated in a 70-nm chromium film was designed for a wavelength of 532 nm and had a wavelength focal length. Then, the ZP relief features were measured on an atomic force microscope Solver Pro P7 (NT-MDT, Russia). From measurements shown in Fig. 1, the relief height was found to vary from 51 to 84 nm, with the average relief height being 67.5 nm and a 5% measurement error. A probe of 10-nm tip radius was utilized. Figure 1 suggests that because of wavelength-long focal length, the ZP is nearly identical to a binary diffractive axicon. That is, starting with fourth-to-fifth zone, the width of all subsequent zones is a bit larger than the wavelength, ranging from 539 to 535 nm.

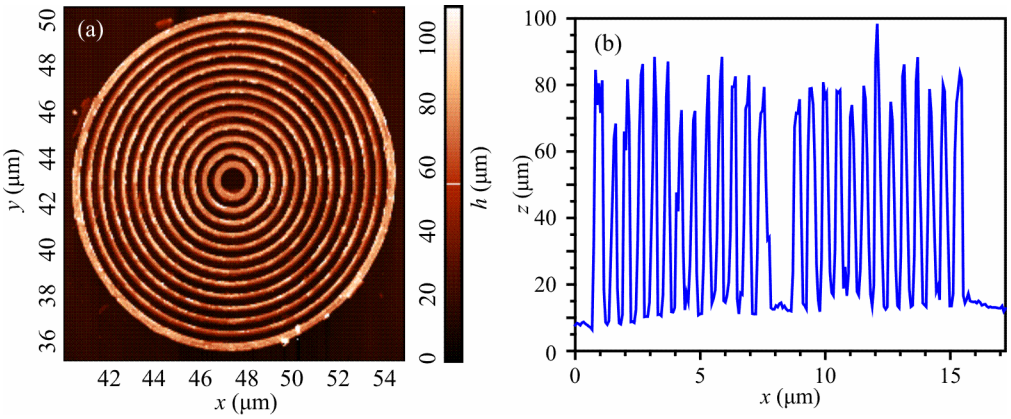

Fig. 1. Chromium ZP: surface relief and y-axis profile measured on an atomic force microscope.

The measured parameters of the ZP relief were utilized in the FullWave software to model the propagation of light using the FDTD method. The simulation parameters were as follows: incident plane wave of length 532 nm, refractive index of chromium $n = 2.66 + 4.16i$ [20], refractive index of the substrate $n = 1.5$, the computation grid step was $\lambda/30$ on all three coordinates, the entire ZP relief was 256×256 pixels, and the incident light was assumed to be linearly polarized. Below, we discuss the results of modeling the propagation of light through the ZP. The incident polarization was assumed to be along the *y*-axis.

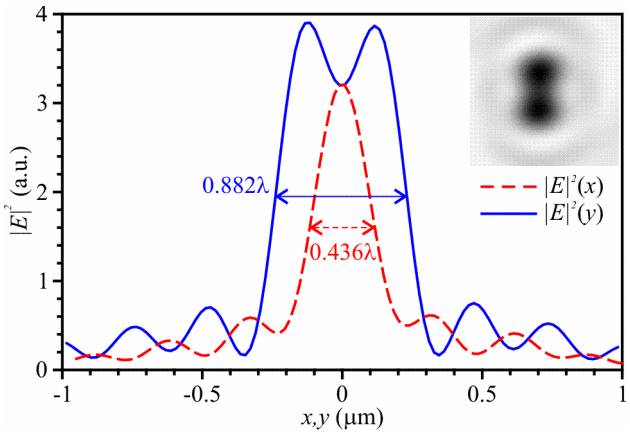

Fig. 2. Simulation results for the ZP in Fig. 1: the intensity profiles are shown along the Cartesian axes.

From Fig. 2, the full width at half maximum of intensity for the electric field $I = I_x + I_y + I_z$ along the *X*- and *Y*-axes is FWHMx=0.436λ and FWHMy=0.882λ. The focusing efficiency, defined as the ratio of the light power coming to the focal spot area limited by the first intensity minimum to the entire incident light power, amounted to $\eta = 5.5\%$. The size of the focal spot was experimentally measured on the Ntegra Spectra (NT-MDT, Russia) unit with a scanning near-field optical microscope (SNOM). The ZP was scanned using a pyramid probe with its square-shaped tip having a 100-nm hole. With such a probe being three-times more sensitive to the transverse *E*-field components than to the longitudinal ones, only transverse *E*-field components were accounted for when numerically simulating the focal spot shape [6]. Figure 3 depicts the numerically simulated focal spot and its profiles contributed to only by the transverse electric field components E_x and E_y ($I_\perp = I_x + I_y$). With the *z*-component being disregarded, although the focal spot is seen to loose its dumbbell shape it is still devoid of

circular symmetry. The focal spot is reduced in size, measuring FWHMx=0.427λ and FWHMy=0.519λ.

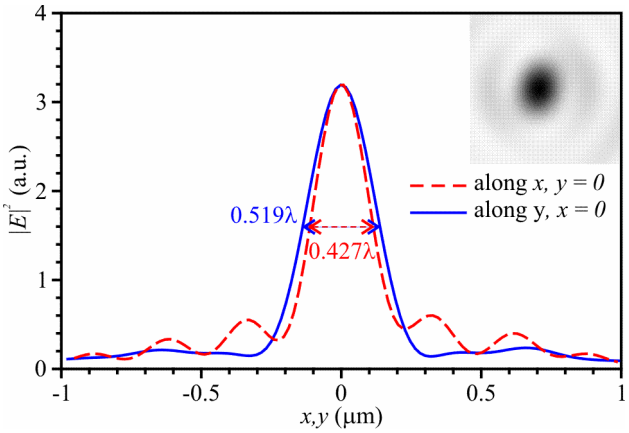

Fig. 3. The intensity pattern produced by the transverse *E*-field components. Intensity profiles along the Cartesian coordinates are also shown.

In this section, by conducting the numerical simulation with due account for the parameters of the fabricated ZP, we showed that when focusing a linearly polarized light, the focal spot measures, for the transverse intensity, FWHMx=0.427λ and FWHMy=0,519λ.

4. Experimental results

The propagation of a linearly and circularly polarized Gaussian beam of wavelength λ = 532 nm through the fabricated chromium amplitude ZP was experimentally studied using an SNOM Ntegra Spectra (NT-MDT). An optical setup used for the SNOM-aided measurements is shown in Fig. 4. Using a lens L_1, the circularly polarized beam (λ = 532 nm) was focused on the substrate. Following the ZP-aided focusing, the transverse intensity distribution in a plane parallel to the ZP was measured at different distances (every 50 nm) with a hollow metal probe *C*. After having passed through the probe, the light was focused by a 100× lens O_1, before traveling through a spectrometer *S* (Solar TII, Nanofinder 30), to filter off the irrelevant radiation, and hitting a recording CCD-camera (Andor, DV401-BV). The circularly polarized beam was generated using a quarter-wave plate.

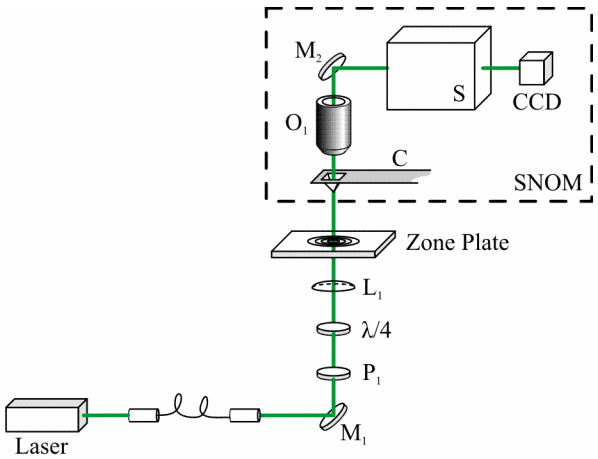

Fig. 4. Experimental optical setup: M_1, M_2 – rotational mirrors, P_1- polarizer, λ/4- quarter waveplate, L_1- focusing lens, C- probe, O_1- microlens, S- spectrometer, and CCD- a CCD-camera.

The result of focusing is shown in Fig. 5. The 2D intensity pattern of the focal spot is shown in Fig. 5(a), with the Cartesian intensity profiles presented in Fig. 5 (b,c) (red crosses denote measured values and a black curve is a cubic-spline interpolation). The SNOM-measured focal spot is located 800-nm away from the surface, the maximal intensity in the focus is 8.5 times the incident beam intensity, with the focal spot measuring FWHMx=(0.47±0.02)λ and FWHMy=(0.48±0.02)λ as it can be seen from Fig. 5. Thus, the resulting near-circular focal spot size is below the diffraction limit ($FWHM_x = 0.51\lambda$), being in a remarkably accurate agreement with the FDTD-aided simulation (FWHM=0.46λ).

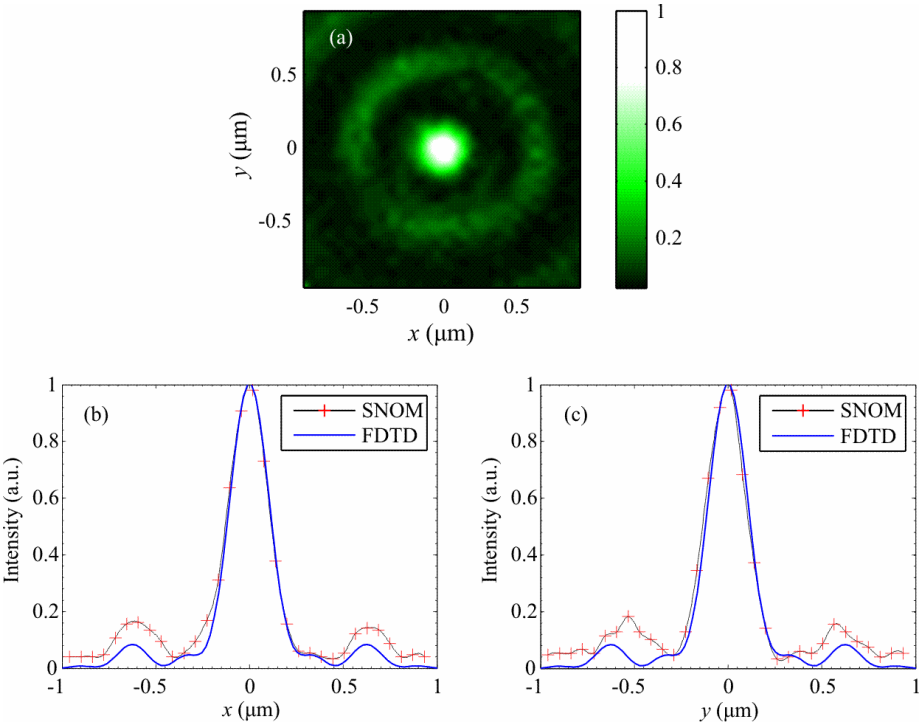

Fig. 5. The intensity profile of the focal spot measured using an SNOM Ntegra Spectra: (a) 2D intensity pattern and intensity profiles along the (b) y- an (c) x- axes. Crosses mark the experimental data and a solid line depicts the cubic-spline-aided interpolation.

Figure 6 depicts the result of FDTD-aided simulation conducted under the experimental parameters of Fig. 5. The profile of the intensity pattern in Fig. 6 is depicted in Fig. 5 (b,c) as a blue curve. The intensity patterns in Figs. 5 and 6 only differ by side-lobes, which are higher in the experiment. The side-lobes in Fig. 5b,c can be explained by the fact that the short-focus ZP in Fig. 1 operates as a diffractive axicon. Meanwhile, the axicon has been known [6,7] to generate a Bessel beam whose side-lobes (observed as peripheral intensity rings around the central intensity maximum) account for 16 percent of the intensity peak.

Figure 7 depicts the experimentally measured intensity pattern and intensity profiles of the focal spot. The experimental data were interpolated using a cubic spline.

Figure 7 shows that when illuminated by a Gaussian beam linearly polarized along the *y*-axis, the chromium binary ZP produces at distance 800 nm a subwavelength elliptic focal spot measuring $FWHM_x = 0.42\lambda$ and $FWHM_y = 0.64\lambda$. The instrument error was 0.02λ. As we showed in Section 3, the numerically simulated focal spot size was obtained with regard for just transverse field components: FWHMx=0.427λ and FWHMy=0.519λ. The deviation of the experimental values from the calculated one is not larger than 1% on the *x*-axis and 20% on the *y*-axis.

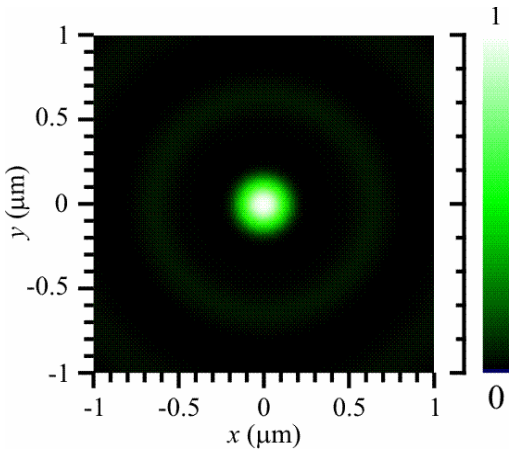

Fig. 6. The calculated 2D intensity of the focal spot

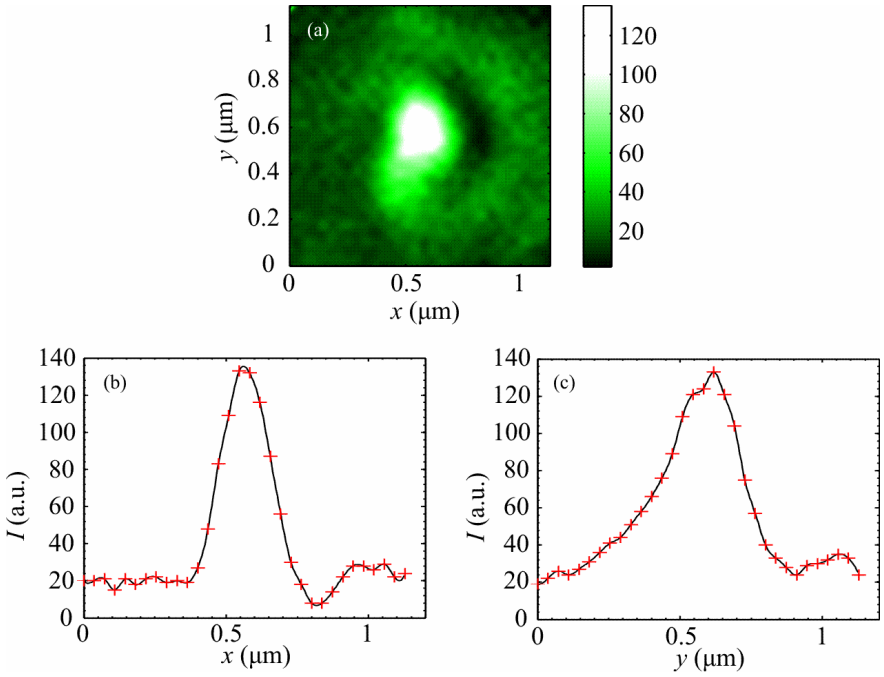

Fig. 7. The intensity distribution of the focal spot measured using an SNOM Ntegra Spectra: (a) 2D intensity pattern and intensity profiles along the (b) *y*- an (c) *x*- axes. Crosses mark the experimental data and a solid line depicts the cubic-spline-aided interpolation.

5. Conclusion

Thus, we have conducted theoretical analysis and experimental characterization of a chromium Fresnel ZP synthesized on a quartz glass, showing it to be able to focus a linearly polarized beam into a beyond-limit focal spot of size FWHM = 0.45λ. The FDTD-aided numerical simulation of a linearly polarized light of wavelength λ=532 nm propagating through a Fresnel ZP has been numerically conducted. We have additionally studied in which way the focal spot parameters depend on the microrelief height, showing heights of 60 and 80 nm to enable an optimal trade-off between the spot's size at FWHM and its maximal intensity.

SNOM measurements have shown that when illuminated by a circularly polarized Gaussian beam, a chromium ZP of relief height 67.5 nm, and incident-wavelength focal length λ produces a circular focal spot of diameter FWHM=(0.47±0.02)λ. Meanwhile, the FDTD-aided numerical simulation gives in this case a round-shaped focal spot of diameter FWHM=0.46λ. When illuminated by a beam linearly polarized along the *y*-axis, the ZP produces an elliptic focal spot of size $FWHM_x$=0.42λ and $FWHM_y$=0.64λ, with the numerically simulated spot measuring $FWHM_x$=0.42λ and $FWHM_y$=0.52λ. The near-accurate agreement between the simulation and experiment suggests that the proposed technique enables simple and low-cost high-NA binary microlenses to be fabricated, using which superfocusing and superresolution imagery can be obtained.

Funding

Russian Scientific Foundation (17-19-01186).